Available online at www.sciencedirect.com
SCIENCE DIRECT®
International Journal of Multiphase Flow 30 (2004) 615–648
International Journal of Multiphase Flow
www.elsevier.com/locate/ijmulflow

Characterization of phase detection optical probes for the measurement of the dispersed phase parameters in sprays

Moongeun Hong [1,*], Alain Cartellier [*], Emil J. Hopfinger

LEGI, Laboratoire des Écoulements Géophysiques et Industriels, (INPG-CNRS-UJF), BP 53, 38041 Grenoble Cedex 9, France

Received 27 May 2003; received in revised form 13 April 2004

Abstract

In order to be able to investigate the characteristics and the spatial evolution of dense sprays produced by coaxial injectors for instance, a measuring technique based on a phase detection optical probe has been developed. Conical optical probes have previously been successfully used in bubbly flows. Aside local concentration, the velocity of gas inclusions was deduced from the analysis of the dewetting time, and, combined with the gas residence time, the bubble size was obtained. Here, it is shown that this technique can also be helpful for the measurements of drop characteristics in dense sprays. Using controlled conditions in terms of drop size, velocity and trajectory, it is demonstrated that for drops above 30 μm in diameter, the velocity and size are evaluated with an uncertainty less than about 15% including variations in the impact conditions. An adapted signal processing has been developed which is shown to be weakly sensitive to the various criteria introduced. When applied to sprays generated by a two-dimensional gas–liquid mixing layer, volumetric fluxes measured by the probe are shown to agree within 15% with a sampling technique. To illustrate the capability of this fairly objective tool, some results are provided and analyzed for the drop velocities and chords as well as for the concentration and the interfacial area density in the near field of dense sprays with a wide size distribution.

Keywords: Dispersed two-phase flow; Sprays; Coaxial injection; Optical probes

* Corresponding authors.
E-mail addresses: Moongeun.Hong@hmg.inpg.fr, conquet@kari.re.kr (M. Hong).
[1] Present address: Korea Aerospace Research Institute, 45 Eoeun-Dong, YouSeong-Gu, Daejeon, 305-333, South Korea.

0301-9322/$ - see front matter © 2004 Elsevier Ltd. All rights reserved.
doi:10.1016/j.ijmultiphaseflow.2004.04.004

1. Introduction

The atomization of liquid jets is a generic situation encountered in various applications such as irrigation or fire fighting water jets, spray painting or coating, metallic beads production, combustion, etc. In order to better understand and to efficiently model such atomization processes, refined experimental data are required on the characteristics of the drops that are formed as well as on the downstream spatial evolution of the sprays (Lin and Reitz, 1998; Lasheras and Hopfinger, 2000). Indeed, depending on flow conditions and nozzle design, different types of interfacial instabilities can be triggered and one key question is to identify the relevant primary atomization mechanisms and to relate them to the resulting drop size. This issue is especially critical for coaxial liquid–gas injectors at large momentum density ratio, such as those used in cryotechnic rocket engines. For these systems, different primary atomization mechanisms have been proposed (see notably Lasheras et al., 1998; Marmottant, 2001; Marmottant and Villermaux, 2003; Varga, 2002; Hong et al., 2002; Yecko et al., 2002; Li et al., 2004) that lead to different scaling laws for the mean drop size. The second issue concerns the spatial development of the spray, involving mechanisms such as dispersion, break-up and coalescence. These effects are often crucial for process optimization. They need to be properly identified in order to improve numerical simulations, and especially those based on kinetic approaches (such as the so-called spray equation Williams, 1985) or on the evolution of some moments such as the interfacial area density (Vallet et al., 2001). So far, drop size and velocity distributions have been mainly measured in the far field of injectors using notably visibility, phase-Doppler and diffraction techniques (see for example Liquid Particle Size Measurement Techniques, 1984). In the near field, where droplets are generally not spherical, imaging techniques have been successfully exploited with regard to drop sizes and velocities, but these are restricted to dilute conditions (see Marmottant, 2001 for example). Aside drop size and velocity, model assessment requires additional dispersed phase characteristics to be measured such as local concentrations, interfacial area densities, joint size–velocity distributions, etc. In addition, measuring techniques need to be developed that can be used in dense conditions, often prevailing in the near injection zone.

Phase detection probes of various types are widely use for the characterization of gas inclusions (Cartellier and Achard, 1991), but these sensors have rarely been employed for drop detection. Sprays often imply high velocities, and therefore optical probes appear to be well adapted since these do not suffer from intrinsic response time limitations compared with alternative phase detection techniques (such as resistive, capacitance, electrochemical or thermal probes). Moreover, considerable progress has been made on probe design (Cartellier and Barrau, 1998a,b), signal processing (Zûn et al., 1995; Barrau et al., 1999), and post-treatment (Liu and Clark, 1995; Kataoka et al., 1986; Cartellier, 1999; Dias et al., 2000). Notably, monofiber optical probes have proved effective for gas inclusions velocity measurements, based on the fact that the dewetting time—i.e. the duration of the liquid–gas transition—is, in most situations, inversely proportional to the interface velocity. Such a feature allows the measurement of various quantities such as size and joint size–velocity distributions, number density, volumetric and number density fluxes, and interfacial area density.

To ascertain the usefulness of optical probes in sprays, the strategy used to develop the technique for bubbly flows was mimicked. In the present paper, the feasibility of drop detection using optical probes is demonstrated by conducting experiments under well controlled conditions in

terms of drop size, velocity and trajectory. These results are presented in Section 3. By analyzing the corresponding droplet signatures, an optimized signal processing has been devised: it is described in Section 4 together with an extensive sensitivity analysis. Finally, in Section 5, measurements undertaken in a high-speed spray produced by coaxial plane jets provide some qualification of the sensor performances in terms of volumetric flux. To illustrate the capabilities of the proposed technique, a few results concerning the evolution of the mean drop size and their implication on primary and secondary atomization mechanisms are also discussed. Before analyzing the probe performances, some general features of the monofiber conical probes are briefly recalled in Section 2.

2. Optical monofiber probe

A monofiber phase detection probe usually consists of a multimode optical fiber with one extremity connected to a Y coupler while the other extremity is immersed in the flow. The light emitted on one arm of the coupler is reflected at the probe tip, and detected through the second arm. This sensor is sensitive to the index of refraction of the fluid surrounding its immersed extremity, and its signal is close to the actual phase indicator function, i.e. the function defined to be unity in one phase and zero in the other one. As recalled in the introduction, optical probes have been significantly improved during the last decade. Concerning their sensing part, current manufacturing techniques ensure a good reproducibility but also, and more importantly, a better control of their shape. In our laboratory, geometry such as simple cones (referred to as 1C—see Fig. 1) or cone–cylinder–cone (referred to as 3C) are currently produced. Although both shapes are suitable for velocity measurements, the conical shape has been selected for spray analysis because it provides smaller sensitive lengths than 3C probes and it is thus better suited for the detection of small drops.

Aside from probe design, a signal processing is required to transform the raw signal into the dispersed phase indicator function. For gas–liquid two-phase flows, the processing has been rendered quite objective (Barrau et al., 1999). Progress has also been made in the post-treatment. Starting from the raw data available, namely the phase indicator function and the statistics of the liquid presence time T_L and the dewetting time T_R, one can deduce the dispersed phase volume fraction α, the joint chord–velocity distribution and the dispersed phase volumetric flux. Introducing some assumptions on the shape and the trajectories of the inclusions (Liu and Clark, 1995; Cartellier, 1999), the joint size–velocity product density $f(\mathbf{x}, d, v)$ relative to inclusion centers can

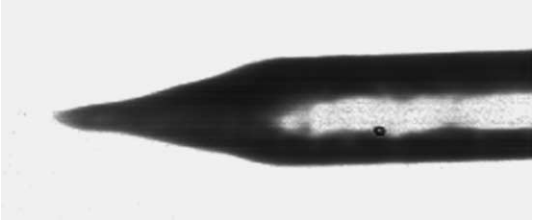

Fig. 1. Image of the tip of a conical optical probe. The fiber O.D. at the right-hand side is 140 μm.

be computed. This function provides a detailed description of dispersed two-phase flows: one can notably extract the number density n (#/m^3) as $n(\mathbf{x}) = \int \mathrm{d}d \int \mathrm{d}\mathbf{v} f(\mathbf{x}, d, \mathbf{v})$, the number density flux φ (#/s m^2) given by $\varphi(\mathbf{x}) = \int \mathrm{d}d \int \mathrm{d}\mathbf{v}\ \mathbf{v} f(\mathbf{x}, d, \mathbf{v})$. The interfacial area density Γ, which is a fundamental parameter in chemical engineering and in combustion, can also be estimated (Kataoka et al., 1986; Cartellier, 1999; Dias et al., 2000; Hibiki et al., 2001). Note, however, that optical probes are sensitive to a single velocity component (namely the velocity component v along the fiber axis) while the full product density involves the velocity vector $\mathbf{v}$: this limitation makes the probes better adapted to unidirectional flows. Monofiber optical probes associated with a specific real time signal processing, have been tested in gas–liquid flows with bubbles above about 1 mm in diameter. The uncertainty on void fraction ranged between −15% and 0% while the uncertainty on gas velocity evolved between −15% and +10% (Barrau et al., 1999). The underestimation on the void fraction was partly attributed to bubbles avoiding the probe. For water drops travelling in air, it can be anticipated that due to the drop inertia, their trajectory should remain unaltered by the presence of the probe (except in the limit of very small droplets). This would suggest that optical probes are less intrusive in sprays than in bubbly flows. The main question concerns, therefore, the actual shape of the signals since the later can be strongly altered by the droplet deformation at impact. So far, applications of optical probes to drop detection have been scarce. A sapphire probe has been used to investigate the sprays produced by a coaxial liquid–gas jet (Carreau et al., 1997). The extremity of this probe is a truncated cone whose flat sensitive tip has a diameter of 90 μm. Such a shape induces large deformations of the drops upon impact (usually, a liquid film forms on its tip), and the minimum, unambiguously detectable droplet size was estimated to be about 120 μm (Porcheron, 1998). Such drawbacks should be avoided with a sharp conical probe. Furthermore, due to its cleaved geometry, this sapphire probe is unable to provide velocity measurements (Cartellier and Barrau, 1998a) and thus it gives access to the dispersed phase fraction and the liquid residence times only.

Fig. 2 illustrates the raw signals delivered by the conical-shaped probe in a dilute region of a spray produced by a coaxial liquid–gas jet. The signal is most of the time at its maximum amplitude, corresponding to the probe surrounded by air. Whenever a drop hits the fiber, the voltage steeply decreases because of the wetting of the probe. The low voltage is maintained while the probe tip remains enclosed by water: the duration of this plateau provides the drop presence time T_L. The transition from the liquid phase to the gas phase (i.e. from low to high voltage) corresponds to the dewetting of the probe. This process occurs within a finite duration T_R from which the drop velocity V is inferred. To determine the relationship between T_R and V, the probes were calibrated on isolated gas slugs produced in an ad hoc experimental test-rig which is described elsewhere (Cartellier, 1990). The transition duration T_R was evaluated as the time between amplitudes corresponding to 10% and 60% (or 70%) of the signal dynamic A_max, defined as the voltage difference between wet and dry conditions ($A_\mathrm{max} = A_\mathrm{G0} - A_\mathrm{L0}$). For the two conical probes used here, denoted by 'a' and 'b' superscripts, the resulting relationships, shown in Fig. 3, are

$$V = 62\, T_\mathrm{R}^{-1.047} \quad \text{for probe}^\mathrm{a}\ (\text{levels}:\ 10\% \text{ and } 60\% \text{ of } A_\mathrm{max}),$$
$$V = 17\, T_\mathrm{R}^{-0.996} \quad \text{for probe}^\mathrm{b}\ (\text{levels}:\ 10\% \text{ and } 70\% \text{ of } A_\mathrm{max}),$$

where V is expressed in m/s and T_R in μs. As already reported (Cartellier and Barrau, 1998a), the rise time is, at first-order, proportional to the inverse of the velocity, indicating that the velocity

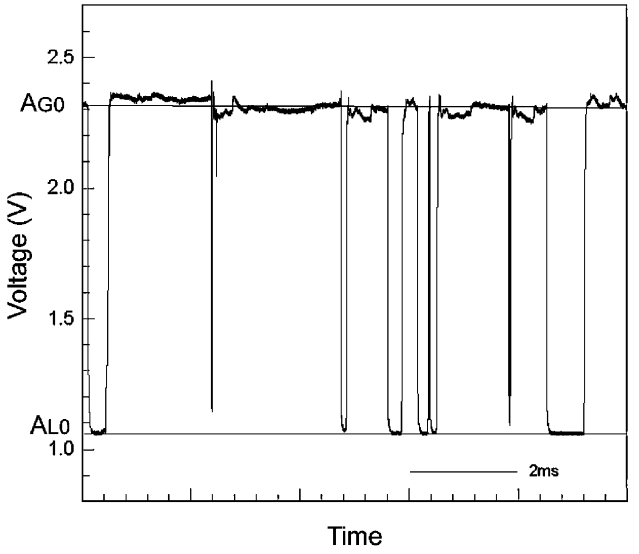

Fig. 2. Raw signal delivered by a conical probe in a spray.

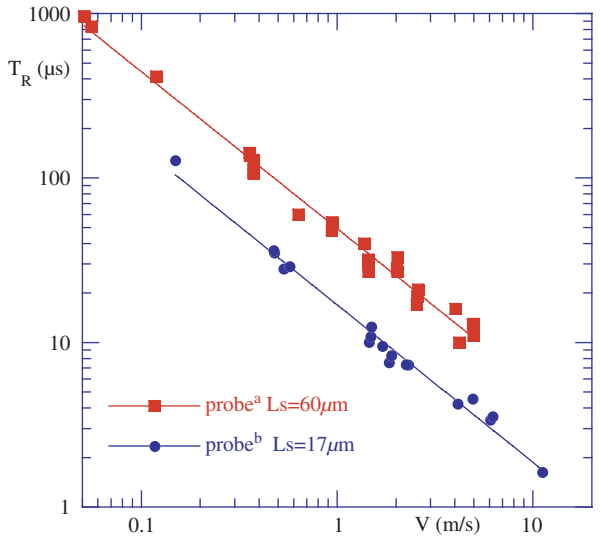

Fig. 3. Rise time versus velocity for the two conical optical probes.

measurement technique is equivalent to a transit time technique counted along some sensitive length of the probe. Yet, deviations from a $V \propto T_R^{-1}$ behavior have been observed either at low velocities (typically below 0.1–0.2 m/s) or for viscous liquids. Here, the calibrations have been achieved between 0.05 and 10 m/s while measurements in sprays (see Section 5) will concern velocities above 0.5 m/s. Therefore, setting the T_R exponent in the V–T_R relationships to -1 induces at most to a 10% uncertainty on the velocity estimate when compared with the best fits. As

discussed in Section 3, this uncertainty is comparable with the dispersion due to trajectory effects, and thus best fits are used for the measurements presented hereafter.

The above relationships determined from the front interface of bubbles will be applied to the rear interface of drops. This is clearly valid for inclusions larger than the probe spatial resolution. For smaller inclusions, the applicability of the T_R–V relationship needs to be checked since the interface deformation and the dewetting dynamic could be sensitive to the inclusion size and to the impact angle. The results presented in Section 3 will demonstrate that the T_R–V relationships stay indeed valid.

In bubbly flows, the upper level that defines the transition duration was typically set to 80–90%. For drops, that threshold has been lowered because the late portion of liquid–gas transitions are significantly slower than their beginning. Indeed, the first portion of the transition corresponds to the dewetting of the cone extremity, while its end corresponds to the interface approaching the base of the cone. The three-phase line becomes longer as time proceeds and the liquid may stick somewhat to the probe due to capillary effects. That feature may explain why the last portions of the liquid–gas transitions are less reproducible than their beginning. Also, after impact, a drop is expected to loose a larger fraction of its initial momentum as time proceeds: this is an extra reason to discard the end of the transitions. Although a detailed analysis of the dewetting would be required to precisely understand the liquid–gas transition features, we choose, for practical purposes, to by-pass this difficulty by discarding the late stage of the transients from the analysis. Indeed, using a somewhat low upper level (say about 60–70%) to define T_R does not induce any limitation provided that T_R is measured with enough resolution. In the present conditions, the electronic response time is about 0.2 μs, so that velocities up to about 40 m/s can be detected with probe[b].

The product $V \times T_R$ represents the magnitude of the sensitive length, L_S, of a given probe, i.e. the length over which most of the dynamics occurs. L_S provides an objective indicator of the spatial resolution (Cartellier, 1990). Despite similar geometry, the change in the prefactors appearing in the T_R–V relationships is probably due to the use of different optical fibers (step index versus gradient index). For probe[a], $L_S = 62$ μm, while it is about 17 μm for probe[b]. These distances are much smaller than the cone length (which is about 200 μm), indicating that the first 60–70 μm for probe[a] (20–30 μm for probe[b]) measured from the tip, provide most of the voltage change. In the following, probe[a] was employed for the analysis of the probe response under controlled conditions (Section 3). In order to detect smaller droplets, probe[b] was used for the experiments performed in coaxial planar jets (Section 5). For the same reason, the sensitivity analysis presented in Section 4 was performed using signals from probe[b].

3. Probe response under controlled condition

To access the dispersed phase characteristics, the raw signal must be processed to extract the arrival time (t_A), the liquid residence time (T_L) and the transition duration (T_R) for each drop impacting the sensor. As shown on the nearly ideal signal of Fig. 4, these data can be evaluated from the four characteristic loci A, B, C, D that will be identified using thresholds on the voltage. These four events are defined as follows:

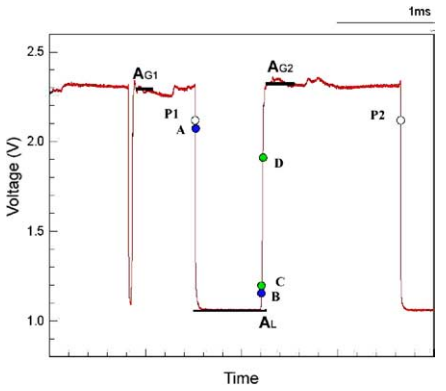

Fig. 4. Typical signature of a large drop with the characteristics events and levels to be detected.

- The very start of the signal fall off from the gas level (event A) corresponds to the entrance of the probe into the droplet. Due to the weak inertia of the gas phase, the droplet is not expected to deform significantly before impact. Besides, the wetting is a fast process, so that gas–liquid transients are very steep. Consequently, the temporal abscissa of the event A, which is also the arrival time for that droplet, is weakly sensitive to the choice of the threshold voltage.
- The very beginning of the signal rise (event B) that follows a plateau at the liquid level corresponds to a probe tip exiting the droplet. However, in that case, the rear interface of the drop is deformed compared to its original shape and the event B does not coincide with the undisturbed interface position. For normal impacts, the difference has been shown to be about a few micrometers (Liju et al., 2001), but it is expected to increase significantly for larger incidence angles.

The liquid residence time T_L is estimated as $t_B - t_A$. The smooth transition from the liquid phase to the gas phase occurs when the probe exits the drop. Its duration T_R is evaluated as $t_D - t_C$ where the events C and D are defined from fixed low and high amplitude thresholds with respect to the maximum signal dynamics. The events C and D are necessarily posterior to the event B, so that the rise time should not be counted in the liquid dwell time. For bubbles the opposite holds since the transition is included in the gas residence time.

Although the above features are physically well grounded, it is necessary to examine the waveform sensitivity to the size, the velocity and the trajectory of the drops in order to elaborate an objective signal processing. Aside accurate drop detection, it is essential to ascertain the validity of the T_R–V relationship for inclusions smaller than the probe sensitive length. In addition, previous experiments performed with bubbles have shown that the dewetting time is sensitive to impact conditions (Cartellier and Barrau, 1998b). More precisely, T_R was found to significantly increase with the incidence angle β between the probe axis and the local normal to the interface (Fig. 5), while the effect of angle γ between the probe axis and the directional velocity of the droplet, is accounted for by the fact that T_R is controlled by the projection of the inclusion velocity along the fiber axis.

To address these questions, controlled piercing experiments have been performed using water droplets produced by the forced Rayleigh breakup of a thin cylindrical jet. Two different needles

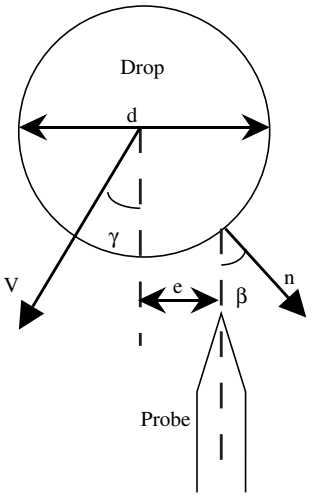

Fig. 5. Probe–drop interaction parameters.

(I.D. $D = 0.25$ and 0.35 mm) were employed to change the jet diameter while the jet velocity was modified by way of a pressurized tank. To force the breakup of the jet at a short distance from the injector, and to control the production of satellite droplets, the injector was connected to a vibrator with an adjustable frequency. The diameter of the droplets evolved from 30 μm for satellite droplets up to 800 μm for the regular drops. Their velocity was varied between 1 and 7 m/s. The probes were located on the jet axis and also off-center in order to change the eccentricity (and thus β). To vary γ, different inclinations were also considered.

To determine the droplet characteristics and the impact conditions, video images were systematically collected during each signal acquisition. The drop size ($d = 2R$), the eccentricity (e), and the angle γ were directly measured on these images. Typical images of the chain of drops interacting with a probe at various eccentricities are given in Fig. 6 with the corresponding raw signals. To determine the reference drop velocity V_{ref}, the distance l between two successive droplets was measured on the images and their arrival frequency f was extracted from the signals delivered by the optical probe. The reference velocity V_{ref} is then given by $f \times l$. The spatial resolution on the images was such that d and V_{ref} were known within 5%. For the smallest drops investigated (i.e. $d = 30$ μm), the uncertainty on the size raised to 15%. Simultaneously, the raw signal from the probe was digitized at a rate between 300 and 600 kHz depending on conditions (higher frequencies were low-pass filtered). Because of the regularity of the signals collected in these conditions, the liquid presence times and the dewetting durations were extracted using the real time signal processing, previously developed for bubble detection (Barrau et al., 1999). Despite the control of the jet breakup by the vibrator, it is difficult to ensure a perfect reproducibility of position and shape of the droplets: fluctuations in positions were about 10% while deviations from sphericity can be as large as 20%. Therefore, instead of performing the analysis for any specific droplet, the measurements have been based on average values. More than a thousand signals and about four images were analyzed for a given condition. The dispersion on the signal dynamics, the velocities and the chords was at most 10%.

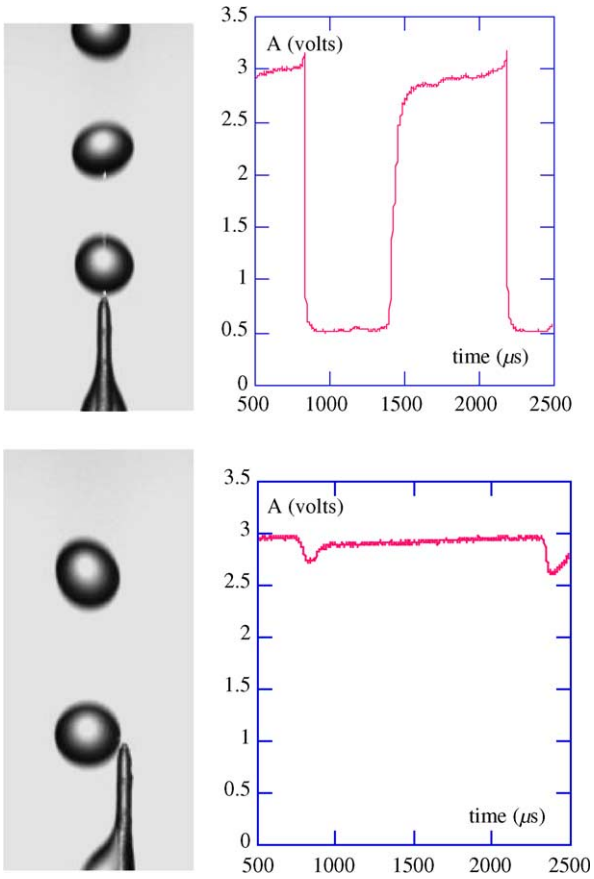

Fig. 6. Train of monodispersed droplets interacting with a conical probe and the corresponding signals ($d \approx 800$ μm, $V_{ref} \approx 1.3$ m/s, top: $e = 0$, bottom: $e = 400$ μm).

Before discussing the probe response, it is worth mentioning that phenomena such as shattering or splitting of the droplets at impact were never observed (the Weber number $We = \rho V^2 d/\sigma$ where ρ is the liquid density and σ the surface tension varied between 10 and 600 in our experiments). The wetting of the fiber is a rather smooth process, mainly due to the sharpness of the probe tip. Additionally, and as anticipated, the drop deformation remained quite limited, notably when compared with the strong flattening observed upon impact on cleaved sapphire probes (Porcheron, 1998).

3.1. Probe response under normal impacts

For normal impacts, defined by $\beta = \gamma = 0$, measurements were conducted for drop diameters ranging from 200 up to 700 μm, and velocities between 1 and 7 m/s. In these conditions, all the liquid to gas transitions span the maximum voltage range available so that all T_R data are eligible for velocity measurements. The mean velocity V detected by the optical probe was found to be within 10% of the reference velocity V_{ref}. The deviations of the mean diameter d, estimated as

$T_L \times V$, from the actual drop size were also less than 10%. Therefore, both size and velocity measurements can be considered as quite good under these conditions.

3.2. Probe response for off-centered impacts

In order to investigate the effect of the impact angle β ($\beta = \sin^{-1} e/R$), the eccentricity, e, was varied by modifying the lateral position of the train of drops with respect to the probe axis. This study has been restricted to velocities directed along the probe axis, and to almost spherical droplets ($\beta \neq 0$, $\gamma = 0$, see Fig. 5). Varying these impact conditions also allows to analyze the detection of small chords cut across a large drop.

The evolution of the signal dynamics with the eccentricity is given in Fig. 7a for various sizes and velocities (see also Fig. 6 and Hong et al., 2000). The ordinate is scaled by the dynamics $A_{e=0}$ measured for a normal impact. Clearly, the signal dynamics is nearly unaffected by the eccentricity, nor by the drop size and velocity as long as $e/R < 0.9$. For eccentricities between $0.9R$ and R, the dynamics is at most reduced by 20%. Therefore, drops are efficiently detected whatever the eccentricity, indicating that the probe response is nearly ideal, i.e. close to the response expected for an infinitely thin sensor. However, for e/R slightly above one, a signal is still perceived although of much weaker amplitude (less than $0.4\ A_{e=0}$). Such signals are due to drops tangentially hitting the conical part of the sensor without wetting the very tip of the probe. Indeed, the maximum displacement for which such tiny signals have been detected is about 80 μm, that is of the order of the optical fiber radius. Such contributions were never observed in bubbly flows because gas inclusions cannot dry the probe under tangential "impact". For drops, the question is whether or not these signals must be taken into account. Since the reconstruction of size or size–velocity distributions involves corrections concerning the probe volume extent for each size class (see Cartellier, 1999 for example) and since these corrections have been established for an ideal probe, it is preferable to discard the events associated with tangential hits from the analysis.

The influence of e/R on the velocity detected by the probe is given in Fig. 7b. The ordinate has been made dimensionless using the velocity $V_{e=0}$ determined under a normal impact. There is a neat decrease of the measured velocity V as e/R increases. As for bubbles, the dewetting time increases with the incidence angle β. However, for bubbles, the sensitivity of T_R to β was so large that a discrimination was introduced in the processing to reduce the uncertainty (Barrau et al., 1999). For drops, no such criterion is needed since the error remains moderate. Indeed, assuming a uniform probability for drop centers, a probe in a monodispersed spray would detect a mean velocity equal to $\int_0^R 2\pi e V(e)\,\mathrm{d}e/(\pi R^2)$. This mean detected velocity has been evaluated from the experimental data of Fig. 7b: it equals $0.8\ V_{e=0}$ for low Weber numbers ($We \approx 13$) and $0.9\ V_{e=0}$ at higher Weber numbers ($We \approx 160$). Hence, in absence of any discrimination on the eccentricity, the averaged measured velocity would be underestimated by 10–20%. As we shall see in Section 5, the experiments performed in high speed sprays indicate that the mean velocity is underestimated by about 10%. This uncertainty is slightly better than the one evaluated from controlled experiments, probably due to the higher impact Weber numbers in the spray conditions.

Finally, the feasibility of chord measurements is demonstrated Fig. 7c. Indeed, all the data do not deviate much from the expected chord for a spherical drop (represented by the solid line).

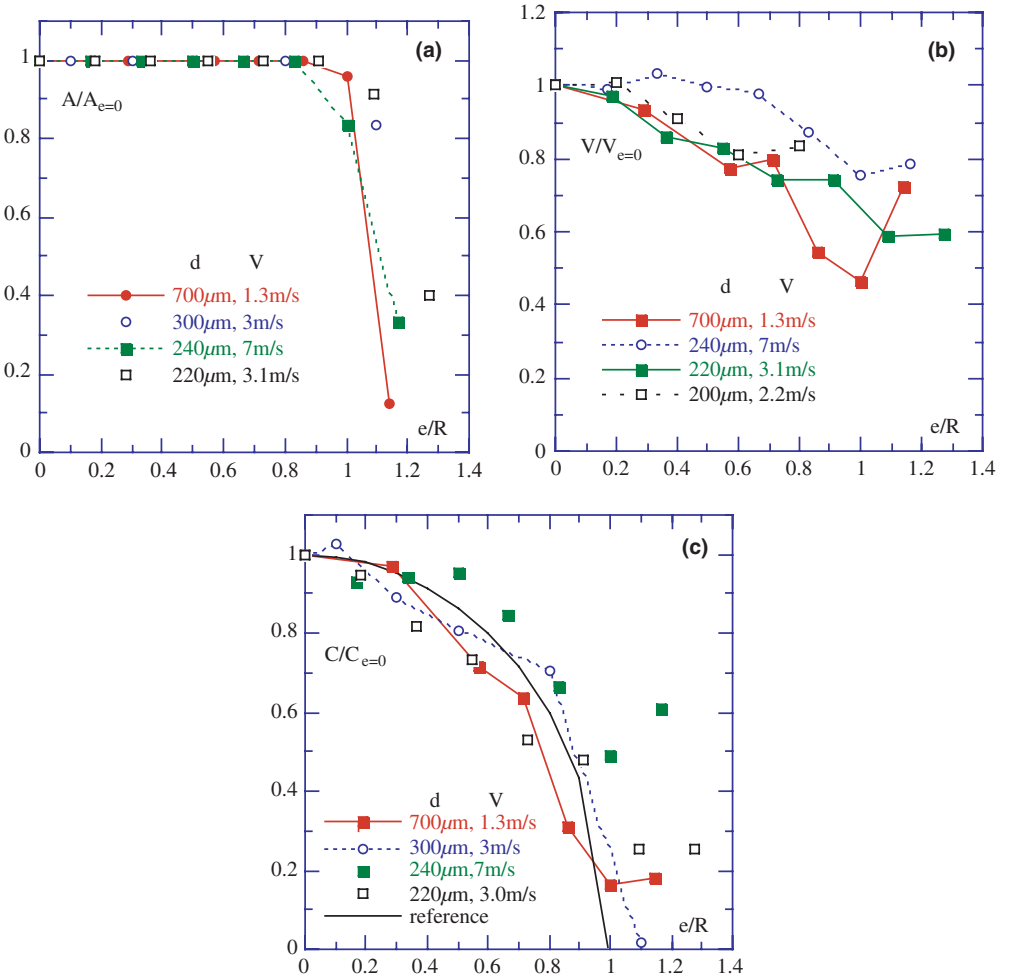

Fig. 7. Evolutions of: (a) the signal dynamics, (b) the detected velocity and (c) the detected chord with the eccentricity for different drop sizes and velocities.

Owing to shape distortions and eccentricity variations experienced by the droplets produced by Rayleigh breakup, the agreement is reasonably good with the exception of the smallest chords ($e/R > 0.9$) which are slightly overestimated. As for bubbles, it happens that the shape distortion partly compensates the error in the velocity measurements, so that the chords are measured within ±10% for e/R less than unity.

For $e/R > 1$, the velocity is not accurate, but more importantly, the error on the chord becomes very large. This is an additional argument in favor of the elimination of signals corresponding to $e/R > 1$. Moreover, such errors cannot be corrected during the post-processing because, when using a single probe, it is not possible to discriminate the eccentricity. Therefore, the only way to get rid of such events is to introduce a selection based on the amplitude. This aspect will be discussed in Section 4.

3.3. Probe response for different inclinations γ

The influence of the angle γ, i.e. the angle between the velocity of droplet and the probe axis, has been investigated for 300 μm droplets at 1.52 m/s only. The probe was inclined while maintaining its tip along the trajectory of the droplet center. In so doing, β always equals γ. As expected, the measured rise time increases with the inclination $\beta = \gamma$. However, when considering the projection of the velocity along the probe axis, the measured velocity remains within 12% of the actual velocity when $\gamma \leqslant 18°$. Hence, the observed deviation has the same magnitude as the one due to the change in the incidence angle β only. Data have also been collected at $\beta = \gamma = 24°$: the detected velocity is then 0.7 times the true velocity projected along the probe axis. Such a deviation is higher than the one due to the change in β only, indicating that the interface deformation upon impact becomes sensitive to γ at large inclinations. Therefore, as a rule of thumb, the velocity is correctly evaluated when the probe axis remains within about ±15° of the main velocity direction of the drops. In practice this constraint is easily fulfilled for jets since the mean velocity has a well defined direction.

3.4. Probe response for various drop sizes d

Although the capability of the probe to detect small chords cut across a large drop has already been demonstrated, it is also necessary to investigate the response of the probe to very small droplets. The satellite droplets have been exploited for that purpose. The signals obtained from probe[a] and under normal impacts have been collected for three drop diameters, namely 30, 70 and 160 μm. As shown by Fig. 8, the signal dynamics is maximum for $d \geqslant 160$ μm, and it decreases significantly for smaller diameters. In particular, for the smallest size considered, i.e. about 30 μm, the signal dynamics was about one third of its maximum. Such a decrease is to be expected from the partial wetting of the sensitive area of the probe. Thus, in principle, a probe of shorter sensitive length should be able to detect smaller droplets. This point has been confirmed using probe[b]

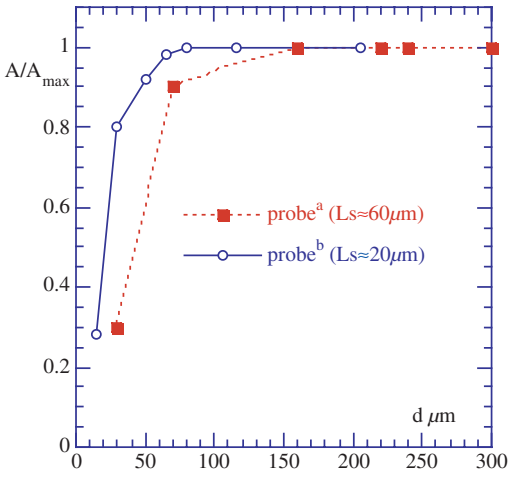

Fig. 8. Evolutions of the signal dynamics upon normal impacts with the drop size for the two probes.

for which L_S is about 20 μm. As anticipated, the decrease in the signal dynamic is much less marked than for probe[a] (Fig. 8). In particular, for $d = 30$ μm, the amplitude is 80% of its maximum for probe[b], to be compared to 30% for probe[a]. Further data were collected for probe[b] in a spray with a narrow size distribution: the amplitude was about 30% for $d = 15$ μm, indicating that such sizes are easily detected.

Another question arises when the probe wetting is incomplete. Indeed, in this case, the dewetting time cannot, in principle, be used to infer the drop velocity. Yet, it is always possible to exploit the transition duration over a smaller amplitude variation (say between levels at 10% and 40% of A_{max} for example). Ideally, one should then refer to a size dependent correlation $T_R\ (V, d)$ to account for the influence of the curvature. But, since the drop diameter remains unknown, such a correction cannot be implemented. Therefore, no attempt has been made to account for a possible effect of the curvature. Instead, it has been assumed that T_R is weakly sensitive to the drop size. This assumption has been checked on actual signals. In Fig. 9 the transition for a 30 μm satellite droplet has been superimposed on the transition for a large drop (200 μm) having almost the same velocity, and it is seen that the transitions have indeed similar slopes. Hence, keeping the calibration as it is, the velocities of small droplets, for which the signal amplitude is a certain percentage of A_{max}, are correctly estimated by assuming that liquid–gas transitions are almost linear, at least at early times. Such a procedure will be further confirmed by the tests presented in Section 4.

Finally, the diameters detected by the probe for small droplets have been compared with their actual value using the reference velocity. The discrepancy was found to be less than a few percent for the 70 and 160 μm droplets, and increases up to 20% for the 30 μm droplets. These magnitudes are of the same order as those obtained for chord detection when varying the eccentricity.

Let us summarize the accessible detection domain of conical probes. No limitation is to be expected at large velocities except for the cut-off due to the electronic response time. Due to droplets sticking on the probe, a limitation is expected at small velocities that should vary with d; it can just be said that the detection boundary is well below 1 m/s for 100 μm droplets. For sizes, no upper limit is expected. The actual lower size limit has not been reached in the present

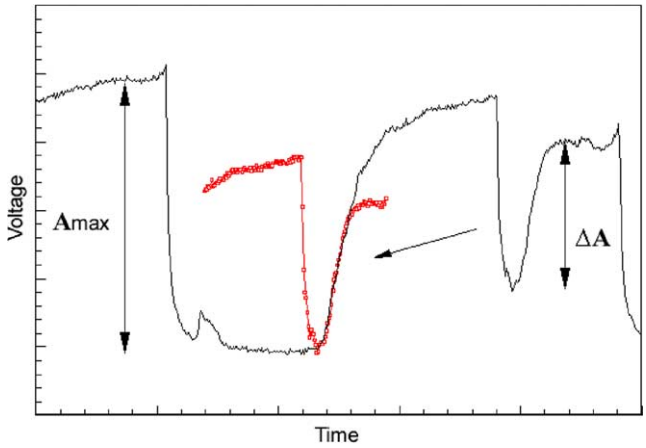

Fig. 9. Comparison of liquid–gas transitions for events of large and small dynamics.

experiments for lack of an adequate spray generator. That limit is clearly below 10–15 μm. Let us also mention that 5 μm droplets were not detected at 0.2 m/s, but were indeed perceived above 1 m/s (see Section 5).

According to the results gathered with controlled probe-drop interactions, the conical probe appears as a promising tool for the characterization of droplets. In particular, the T_R–V relationship established on large inclusions has been found valid over a broad range of drop size (including sizes smaller than the probe latency length) and impact conditions. Although the uncertainties on size and velocity are typically about 10–20% and thus are somewhat higher than for techniques such as phase-Doppler anemometry, the probe technique is not restricted to spherical inclusions nor to dilute sprays.

4. Signal processing and sensitivity analysis

The determination of the A, B, C, D events for every drop signature relies on a shape analysis which introduces some adjustable coefficients. Since the criteria introduced for bubble detection ended in objective and reliable procedures (Barrau et al., 1999), the same principles were applied to drop detection. However, some modifications were required to account for specific aspects of the response of optical probes in sprays. In particular, in bubbly flows, the signal amplitude for a probe entirely immersed in the liquid phase, (A_L), remains stable, and this continuous phase voltage was used as the reference level. In sprays, the continuous phase level (A_G) that corresponds to a probe immersed in the gas, is not as stable as the liquid level in bubbly flows. The time evolution of the gas level, clearly visible in Fig. 4, is due to the partial and/or progressive dewetting of the probe sensing tip that occurs between successive drop impacts. Variations of A_G are enhanced as the droplet inter-arrival time decreases, i.e. as the drop concentration and/or their velocity increases. Also, the carrier phase turbulence could affect the wetted area, and it is partly responsible for gas level fluctuations. Here, the liquid level cannot be used as an alternate reference since, as shown in Section 3.4, the signal dynamics vary with the droplet size. In such circumstances, it is therefore mandatory to scrutinize the time evolution of the amplitudes corresponding to each phase, a feature that renders the detection procedure more complex. In addition, a real time processing was discarded because of the high sampling rates, often as large as a few MHz, required for the detection of droplets generated in atomizers. Instead, the signals were stored and subsequently processed.

In the following, the whole procedure is first described in detail, and the sensitivities of the measured quantities to the various coefficients introduced in the signal processing are then quantified and discussed.

4.1. Signal processing

The correct identification of A, B, C, D events for any given droplet requires the evaluation of the reference gas and liquid voltages in the neighborhood of each drop signature. Such an operation cannot be undertaken before having located these signatures, and to circumvent this problem, the detection has been split into two steps. The first step makes use of "average" gas and liquid levels, defined over the whole duration of the record, while the second step relies on "local"

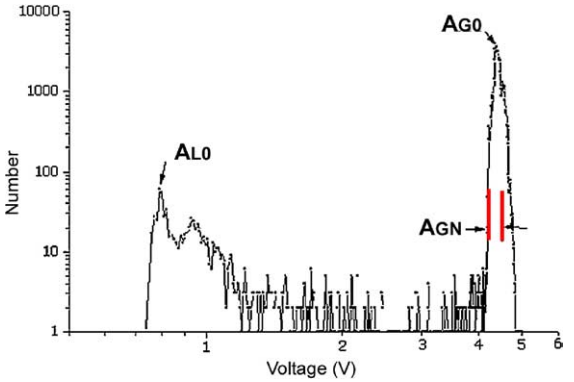

Fig. 10. Typical amplitude histogram and definition of reference levels.

phase levels as detailed in Section 4.1.3. Considering average levels is meaningful because, despite strong fluctuations, the gas and the liquid voltages evolve within well defined boundaries. This is clearly seen on the amplitude histogram of Fig. 10 performed on a 10″ signal collected in the planar mixing layer (see Section 5). From such histograms, the "average" gas A_{G0} and liquid A_{L0} levels are defined as the abscissa of the two side peaks. In addition, the amplitudes of the fluctuations around the averages, noted A_{LN} and A_{GN}, respectively, are estimated as twice the amplitude difference between the foot of the each peak and the corresponding maximum (Fig. 10).

4.1.1. First drop detection step

The reference levels A_{G0} and A_{L0} are used for the identification of a first set of drops. A droplet is detected in the vicinity of a point P_1 (see Fig. 4), whenever the amplitude of the signal becomes less than the threshold $A_P = A_{G0} - C_{L1}(A_{G0} - A_{L0})$. C_{L1} is a security coefficient accounting for the gas phase level fluctuations. In bubbly flows, the detection criterion involved the noise at the liquid level because of the high stability of the later. Here, the amplitude difference $A_{G0} - A_{L0}$ is used instead, in order to avoid interpreting fluctuations or slow variations of the gas level as a droplet signature. The default value of C_{L1} is set to 0.2. The above threshold is applied over the whole record: on the example of Fig. 4, the next drop is detected at P_2. Every intervals $[P_1, P_2]$ between successive droplets are then analyzed a second time in order to perform two operations, namely the evaluation of "local" liquid A_L and gas A_{G2} levels (see Fig. 4), and the detection of low amplitude signatures that were missed during the first detection.

4.1.2. Evaluation of local phase levels

The gas level A_{G2} is required to measure the duration of the liquid to gas transition (the gas level has been indexed by 2 because it corresponds to a portion of signal following the drop under analysis). To respect the procedure employed during probe calibration, A_{G2} is evaluated as the mean value of the gas level over a short duration, taken just after the liquid–gas transition has been completed (Fig. 4). That duration is a fraction of the time interval between successive droplets. The later is evaluated between the point of amplitude $A_{G0} - A_{GN}/2$ located at the end of the liquid–gas transition of the first drop and P_2 (Fig. 4). To minimize the influence of the gas level fluctuations, the selected fraction must be small enough: the default value is set to 10%.

For the local liquid level, A_L, two cases need to be distinguished. For a drop large enough to wet the entire sensitive part of the probe, the bottom of the signature takes the form of a plateau. A_L corresponds to the average amplitude of this plateau (Fig. 4): it is estimated between the couple of events of amplitude $A_{L0} + A_{LN}/2$ framing the plateau. Note that this quantity happens to be fairly stable from drop to drop. For small drops or chords, the sensitive part of the probe is only partly wetted. The corresponding signals do not exhibit any plateau but just a local minimum (whose amplitude is always higher than the plateau level because of the partial wetting). In that case, A_L is defined as the minimal amplitude, either using the absolute minimum or an average evaluated in the close vicinity of the minimum to avoid spurious fluctuations.

4.1.3. Second drop detection step

The first procedure does not allow to detect droplets whose dynamic is less than C_{L1} $(A_{G0} - A_{L0})$. The detection of finer droplets or smaller chords is undertaken in each interval $[P_1, P_2]$, using a new threshold based on the local gas level A_{G2} and on the magnitude of the gas level fluctuations. In so doing, the detected droplets are not mistaken with slow evolutions of the gas level, nor with its fluctuations. This new threshold is defined as $A_{G2} - C_{L2} \times A_{GN}$. C_{L2} should be higher than 0.5 to get rid of most of the noise: its default value is set to 1.2. Note that, introducing the signal to noise ratio $\mathrm{SNR} = (A_{G0} - A_{L0})/A_{GN}$, this is equivalent to a threshold $A_{G2} - (C_{L2}/\mathrm{SNR}) \times (A_{G0} - A_{L0})$. Hence, the second detection step becomes active compared with the first provided that $C_{L2}/\mathrm{SNR} < C_{L1}$. The criterion used in this second step implies that any fall in the signal of less than the above threshold is considered as a gas level fluctuation. This threshold also allows to eliminate most signals due to tangential hits at eccentricities exceeding the drop radius. Yet, the discrimination between short pulses due to tangential hits from pulses due to very small droplets remains imperfect. To discuss that point, the evolution of the signal dynamics with the drop size must be put in perspective with its evolution with the eccentricity. Although data are lacking to form a complete picture of the function $A(e, d)$, it is clear from Figs. 7a and 8 that discriminating the impacts such that $e/R > 1$ using an absolute amplitude can interfere with the detection of small droplets. The amount of misinterpretation depends on the extent of the size distribution. If the later consists of drops large enough for the dynamics to remain at its maximum, them the discrimination would be efficient. But, whenever drops are small enough for the dynamics to drop off, the ambiguity cannot be avoided. Drops below about 50 μm are commonly found in atomization processes, and thus some amount of ambiguity is to be expected in most situations (at least for the probes used here). The resulting distortion, evaluated from a sensitivity analysis, will be discussed in Section 4.2.

At this stage, all drops hits have been detected (within the limit mentioned above) and for every signature, the local liquid level (A_L) and the local gas level (A_{G2}) following the hit are known. When applying the procedure to the whole signal, the quantity A_{G1} which is the gas level following the previous drop (Fig. 4) is also available for every hit (except the very first event of a record for which A_{G1} is set to A_{G0}).

4.1.4. Evaluation of the liquid presence time

The local phase levels being determined, the events A and B are localized at the amplitudes $A_{G1} - C_{S1}(A_{G1} - A_L)$ and $A_L + C_{S2}(A_{G2} - A_L)$, respectively. Note that, although A_{G1} may not be truly representative of the gas amplitude before a hit, its use for the detection of type A events is

inconsequential because gas–liquid transitions are very steep. For the (smaller) droplets detected during the second step, A_{G1} is replaced by A_{G2}. The coefficients C_{S1} and C_{S2} are adjustable: their default values are 0.2 and 0.1, respectively. For a more accurate detection of B events, it is recommended to reduce the coefficient C_{S2} down to values compatible with the noise level, namely such that $C_{S2}(A_{G2} - A_L) > A_{LN}/2$. This step provides the drop arrival time and the liquid presence time.

4.1.5. Evaluation of the dewetting time

During the probe calibration, the rise time–velocity correlation is established from full liquid to gas transitions, i.e. for probe tips that are fully wetted before the start of the transient. Consequently, for all the signals with a maximum dynamic (and which have been identified during the first detection step), the velocity is directly inferred from the rise time. The later is evaluated as $t_D - t_C$ where the events C and D correspond to amplitudes equal to $A_L + C_c(A_{G2} - A_L)$ and $A_L + C_d(A_{G2} - A_L)$, respectively. The lower C_c and upper C_d thresholds are the same as those selected during the calibration (typically $C_c \approx 0.1$, $C_d \approx 0.6 \sim 0.7$). In contrast with bubbles, the dynamic is weakly affected by the eccentricity and no selection criterion has been introduced on the dwell time.

The above procedure concerns but the largest drops. In most sprays, a significant portion of the drop size distribution is located below the probe latency length (that is typically about 20–50 μm) so that considering only the signatures with a maximum dynamic drastically restricts the fraction of droplets eligible for velocity measurements. To increase this fraction, it has been assumed that, for a given velocity, the signal from a drop smaller than the latency length corresponds to a portion of a full amplitude signature, as shown Fig. 9. In other words, since liquid to gas transitions are nearly linear over a significant range of thresholds (as shown in Cartellier and Barrau, 1998a), the liquid to gas transition in case of partial wetting is shortened in proportion of the decrease in the dynamic. This assumption is sustained by the fact that meaningful velocity measurements were successfully performed on small droplets under controlled experiments (see Section 3). Therefore, a partial rise time t_R is first estimated. Then, t_R is transformed into an equivalent rise time T_R for a full dynamic according to a linear extrapolation: $T_R = (\Delta A/A_{max})t_R$, where A_{max} is the maximum signal dynamic and ΔA denotes the partial dynamic considered. The drop velocity is then deduced from T_R using the calibration relationship. Such a procedure is not applicable to very weak signals. First, the later can correspond to the final portion of liquid–gas transitions which are both non-linear in time and quite slow: such situations are eliminated from the choice of the upper threshold C_D. Small signals can also correspond to large eccentricities for which the velocity measurement is not accurate as shown in Section 3. To eliminate these situations, the above procedure is applied to signals of sufficient amplitude. More precisely, the liquid level must fall at least down to $A_A = A_{L0} + C_V(A_{G0} - A_{L0})$, and the coefficient C_V allows to tune the minimum signal dynamic for which velocity measurement are achieved. Its default value is 0.5. This selection criterion is imperfect since it also discards some meaningful signals from tiny droplets. This defect is unavoidable since the signal processing is unable to distinguish between a small droplet and a small chord cut through a large inclusion. However, the resulting error is strongly dependent on the probe latency length. Indeed, the smaller L_S, the smaller the droplet size for which the dynamic reaches the above threshold. For $L_S = 20$ μm, an extrapolation of the results of Fig. 8 implies a cut-off at a size about 10–15 μm while eccentricities above 1.1 are efficiently eliminated (for $C_V = 0.5$).

At this stage, the liquid presence time for all the detected droplets and the dewetting time are available for all droplets whose signatures drop below the level A_A. Both velocity and chord are therefore measured for each of these signatures, which are referred to as direct detection in the sequel. In contrast, no velocity measurement and thus no chord estimate are available for signals with a dynamics less than A_A.

4.1.6. Evaluation of chord and velocity for low amplitude signals

In bubbly flows, a velocity was attributed to low amplitude signatures during the post-processing phase. The procedure was based on a time interpolation between available measured velocities (i.e. those resulting from the so-called direct detection), the reason being that bubbles are imbedded in an inert carrier phase so that strong velocity jumps are not to be expected between successive inclusions (at least for narrow size distributions). In turbulent mist flows, such an interpolation is much less valid because of droplet inertia. Instead, strong fluctuations in velocity are to be expected even over short time intervals. A different procedure was therefore implemented to evaluate the chord and the velocity associated with low dynamic signals. Unfortunately, it has not been possible to elaborate a procedure grounded on an indisputable basis. Instead, by examining joint chord–T_L plots (Fig. 11), a strong correlation can be identified between these two quantities. It has been therefore assumed that the mean trend, extracted using a power law $C = aT_L^b$ adjusted for each set of measurement, can be applied to low amplitude signals. Velocities for small T_L are then estimated as C/T_L. This is equivalent to introducing a mean chord–velocity correlation, but only valid for the smallest intercepted chords. By no means does this statement imply that a size–velocity correlation holds for the entire population. The proposed procedure, although unsatisfactory, provides a way to weight the relative importance of these "small signals"

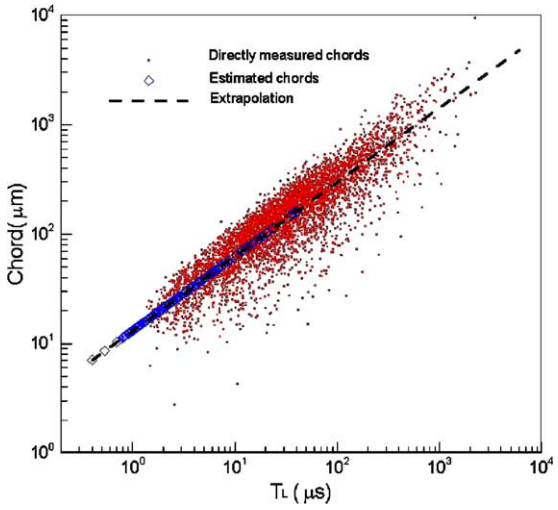

Fig. 11. Typical correlation between liquid dwell times and measured chords as observed in the coplanar gas–liquid jet at $x/D = 1.5$, $y/D = 0.5$ for $U_G = 40$ m/s, $U_L = 0.35$ m/s. The resolution on T_L is about 0.4 μs. The extrapolation procedure concerns T_L smaller than about 2 μs.

with respect to the size distribution and the volumetric flux, and thus it allows to check the quality of the measurements. This aspect will be discussed in more detail in Section 5, but the impact of the above procedure would be minimized as the proportion of direct detection increases. Although that proportion varies with flow conditions (by the way of the size distribution), it is maximized when using optimized detection criteria and probes of small sensitive length. This is illustrated by the data of Fig. 11 obtained with probe[b] in the planar mixing layer i.e. in presence of a wide size distribution. No direct velocity estimate is available for liquid dwell times less than about 1.2 μs, but the success rate (i.e. the proportion of direct detection) is close to 90%.

4.2. Sensitivity to the processing criteria

The importance of optimized detection criteria has been emphasized in the previous section. In addition, the signal processing must be as objective as possible to provide reliable measurements. This section is therefore devoted to a sensitivity analysis to the various coefficients that have been introduced. Table 1 summarizes their respective role in the detection procedure.

All the coefficients (except C_{L2}) evolve between 0 and 1, but they cannot vary freely because they are limited by considerations related with the physical origin of the drop signatures.

- The coefficients C_{L1} and C_{L2}, used during the two detection steps, should be kept as low as possible to identify all the droplets impacting the drop. However, too low values lead to interpret the noise or the fluctuations at the gas level as liquid inclusions. In particular, if C_{L1} is too low, there is some risk to badly interpret low frequency modulations of the gas level. For C_{L2}, higher frequency fluctuations could be confused with droplets. Because the signals are analyzed twice, the droplets missed by a too large value of criterion C_{L1} during the first step, can be detected by a more strict criterion C_{L2} (Fig. 12). These coefficients essentially control the hit detection.
- The fraction of time intervenes in the estimation of the local gas phase level. All the A, B, C, D events are therefore indirectly affected by this parameter. Its effect is strongly connected to the more or less fluctuating nature of the signals, and is thus difficult to appreciate its influence in general terms.

Table 1
Adjustable coefficients and their influence on the various quantities extracted by the signal processing

Detection	Criteria	Coefficients/default values	Comment, constraint
First detection step, $P_{1,2}$ Local gas level, $A_{G1,2}$ Local liquid level, A_L	$A_{G0} - C_{L1}(A_{L0} - A_{G0})$	$C_{L1} = 0.2$ *Time fraction* = 0.1	
Second detection step	$A_{G2} - C_{L2}A_{GN}$	$C_{L2} = 1.2$	Active if $C_{L2}/\mathrm{SNR} < C_{L1}$
Drop entry, A	$A_{G1} - C_{S1}(A_{G1} - A_L)$	$C_{S1} = 0.2$	$C_{S1} > 1/(2SNR)$
Drop exit, B	$A_L + C_{S2}(A_{G2} - A_L)$	$C_{S2} = 0.1$	Minimum recommended $C_{S2} \approx A_{LN}/[2(A_{G0} - A_{L0})]$
Direct velocity detection	$A_{L0} + C_V(A_{G0} - A_{L0})$	$C_V = 0.5$	
Start rise time, C	$A_L + C_C(A_{G2} - A_L)$	$C_C = 0.1$ typical	Set from the calibration
End rise time, D	$A_L + C_d(A_{G2} - A_L)$	$C_d = 0.7$ typical	Set from the calibration

The amplitudes A_{G0}, A_{L0}, A_{GN} and A_{LN} are determined during the initialization, and $\mathrm{SNR} = (A_{G0} - A_{L0})/A_{GN}$.

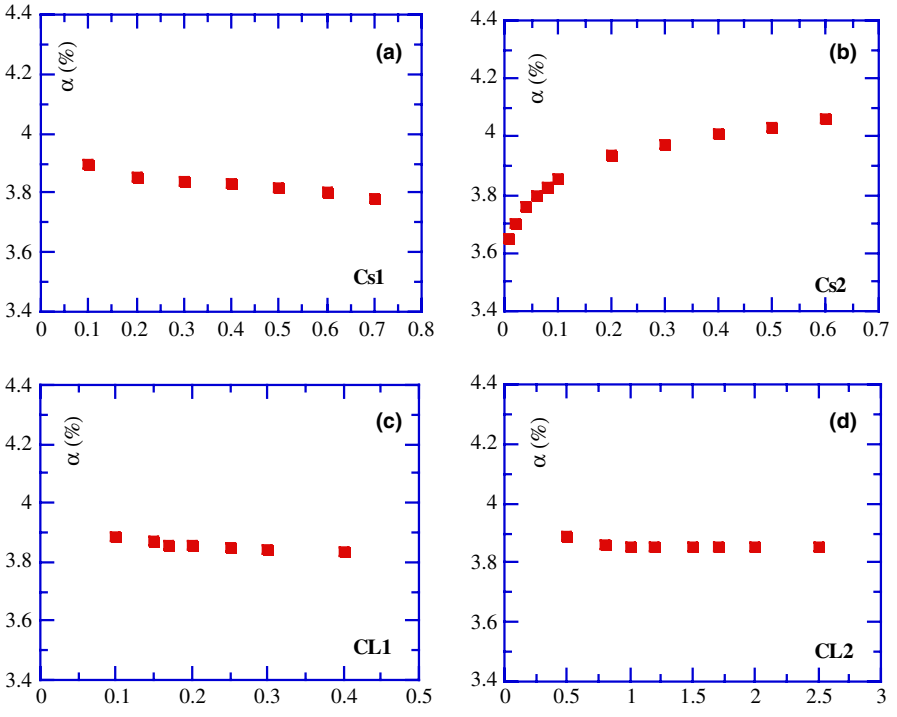

Fig. 12. Sensitivity of the dispersed phase fraction to the processing coefficients: (a) C_{S1}, (b) C_{S2}, (c) C_{L1} and (d) C_{L2}.

- The coefficients C_{S1} and C_{S2} define the entrance (event A) and exit (event B) of the probe in a drop. The physics of the probe/drop interaction dictates that the event A must be close to the gas plateau level and the event B should be located just after the liquid level. Therefore, C_{S1} and C_{S2} should be as small as possible, but still compatible with the noise levels.
- The coefficient C_V defines the limit in the dynamic for direct velocity measurements. It does not affect the liquid presence time, nor the liquid fraction.

As it was done for bubbly flows (Barrau et al., 1999), the sensibility of concentration, size and velocity measurements to these coefficients has been analyzed. For this purpose, use has been made of the signals delivered by the optical probe located in the near (dense) region of a coaxial planar jet (see Section 5). The sampling rate was fixed to 5 MHz. With the optical probe[b], typically about 6000 hits were detected within 10 s. In addition, the size distribution was very large, the chord pdf ranging between less than 10 up to 900 μm (see Fig. 16). These stringent conditions are therefore well adapted for a test of the proposed signal processing.

4.2.1. Liquid fraction

The local liquid fraction (or local concentration) is evaluated as $\alpha = \sum_i T_{Li}/T_t$, where T_{Li} represents the residence time of the inclusion i on the probe and T_t is the total duration of the measurement. The summation is achieved over all inclusions detected during T_t For the same record, the Fig. 12 provides the evolution of the liquid fraction with the coefficients C_{S1}, C_{S2}, C_{L1},

and C_{L2}. For each curve, the coefficients except the one used as the abscissa, were fixed to their default value, namely $C_{S1} = 0.2$, $C_{S2} = 0.1$, $C_{L1} = 0.2$, $C_{L2} = 1.2$ and a 10% time fraction for the determination of A_{G2}.

The sensitivity to C_{S1} is very weak, the variations in the liquid fraction being lower than 2% (in relative value). That weak sensitivity is in agreement with the rapid wetting of probe. The sensitivity to C_{S2} is, as expected, much more marked. Indeed, the transition during the dewetting is much slower than for the wetting, and as C_{S2} grows, a larger fraction of the liquid to gas transition is taken into account in the liquid presence time. As previously said, the physics of the probe–droplet interaction dictates that this transition must not be included in the drop dwell time, so that choosing C_{S2} above 0.1–0.2 is incorrect. However, even when setting C_{S2} to 0.5, the overestimation in the concentration is less than 5% (in relative value): this is still not unreasonable and demonstrates that the processing is moderately sensitive to C_{S2}. In the lower limit, the concentration decreases with C_{S2} but it remains within acceptable limits (4–5%) even when the threshold in amplitude goes below the noise at the liquid level. The sensitivity to C_{L1} is very weak, although one can detect a small increase in α at low values ($C_{L1} < 0.15$). This increase is partly due to the fact that fluctuations of the gas level start to be misinterpreted as the presence of the liquid phase, and also because more and more tangential hits contributions are included in the estimation of the concentration. Similar considerations hold for the coefficient C_{L2} used during the second detection step. C_{L2} has been varied from 0.5 up to 2.5. The results of Fig. 12 have been obtained for an SNR about 5.6, so that in terms of the absolute threshold $A_{G2} - (C_{L2}/\mathrm{SNR}) \times (A_{G0} - A_{L0})$, C_{L2}/SNR evolves from 0.08 to 0.45. For C_{L2} above 1.1, C_{L2}/SNR is higher than C_{L1} and the sensitivity is zero since the second detection step becomes inactive. For C_{L2} between 0.5 and 1.1, the relative variation in the concentration is at most 2%. These weak sensitivities to the detection thresholds demonstrate that, although the processing is unable to discriminate tangential hits from small droplets, the contribution of tangential hits to the concentration remains negligible and the proposed procedure is reliable.

According to the above results, and provided that the physics of probe-drop interactions is correctly taken into account, the proposed signal processing is poorly sensitive to the selection criteria, and gives thus a fairly objective measure of the dispersed phase concentration.

4.2.2. Velocity and chords measurements

Various velocities can be evaluated from the data extracted from optical probes. For the purpose of the sensitivity analysis, use has been made of an average velocity defined as the arithmetic average of the detected velocities. Although such a velocity is not representative of the volumetric flux, it is a good indicator to test the signal processing. Two estimates of the average velocity are considered in the following. First, $\langle V_d \rangle = \sum_{i=1\ldots N_d} V_{di}/N_d$ denotes the average velocity of the N_d droplets whose velocities V_{di} have been directly measured, that is without considering the smallest liquid dwell times. Second, the average velocity $\langle V_e \rangle$ including the extrapolation procedure introduced for the smallest liquid dwell times is given by $\langle V_e \rangle = (\sum_{i=1\ldots N_d} V_{di} + \sum_{j=1\ldots N_e} V_{ei})/N_t$, where N_e is the number of droplets whose velocity is estimated by extrapolation (i.e. $V_{ei} = C_i/T_{li}$) and where $N_t = N_d + N_e$ is the total number of detected droplets. Let us recall that a direct evaluation of the velocity is performed for the signatures reaching the amplitude $A_A = A_{L0} + C_V(A_{G0} - A_{L0})$, or equivalently for events with a dynamic equal or higher than $(1 - C_V)\ A_{max}$. Thus, direct velocity measurements are performed over more and more

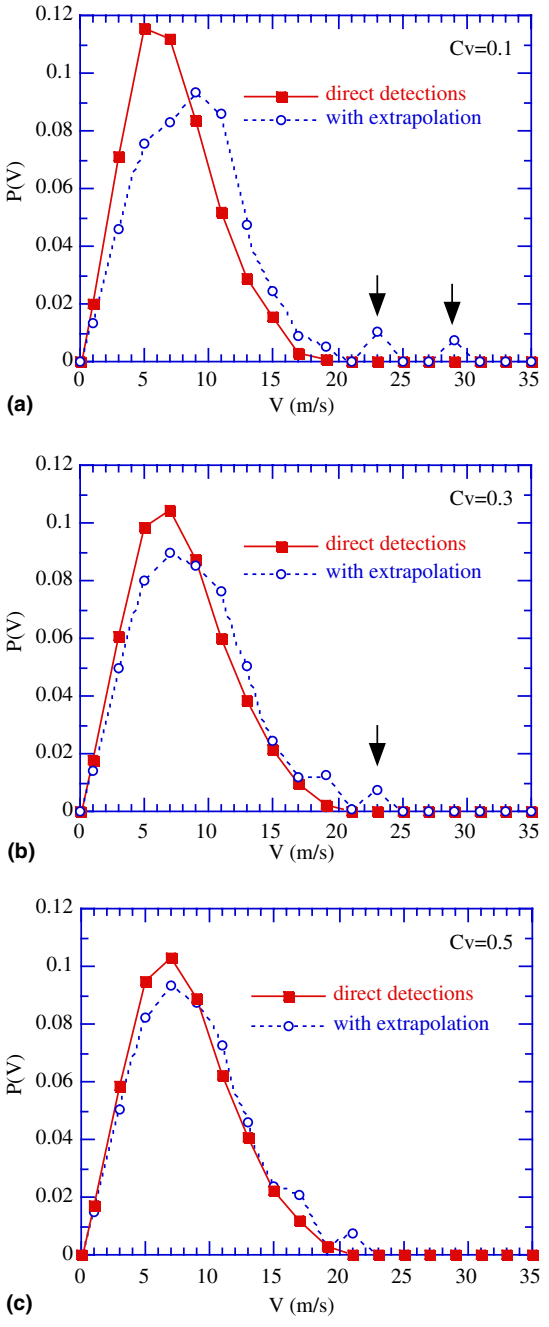

Fig. 13. Velocity distributions with and without the extrapolation procedure for different amplitude thresholds C_V.

droplets as C_V increases. The influence of C_V on the measured velocity distributions both with and without extrapolation is illustrated Fig. 13. The main difference between the distributions comes

from a few realizations at high velocities (indicated by arrows in Fig. 13), that become more numerous as C_V decreases. These realizations originate from the extrapolation procedure, and they are due to the smallest chords (or liquid dwell times) present in the record. Such abnormal events almost disappear for C_V about 0.5 and the velocity distributions with and without extrapolation become almost the same in these conditions.

To quantify the effect of C_V, the average velocities $\langle V_d \rangle$ and $\langle V_e \rangle$, scaled by $\langle V_d \rangle$ evaluated for $C_V = 0.5$, are compared in Fig. 14a. On that example, $\langle V_d \rangle$ first increases with C_V before reaching a plateau. This is because the data have been collected in the near region of the injector where small droplets are faster than the larger ones, and, as C_V grows, more and more small droplets are taken into account in the velocity estimate. On the other hand, $\langle V_e \rangle$, decreases slightly with C_V because the extrapolated velocities decrease with C_V. The important point is that the sensitivity to C_V

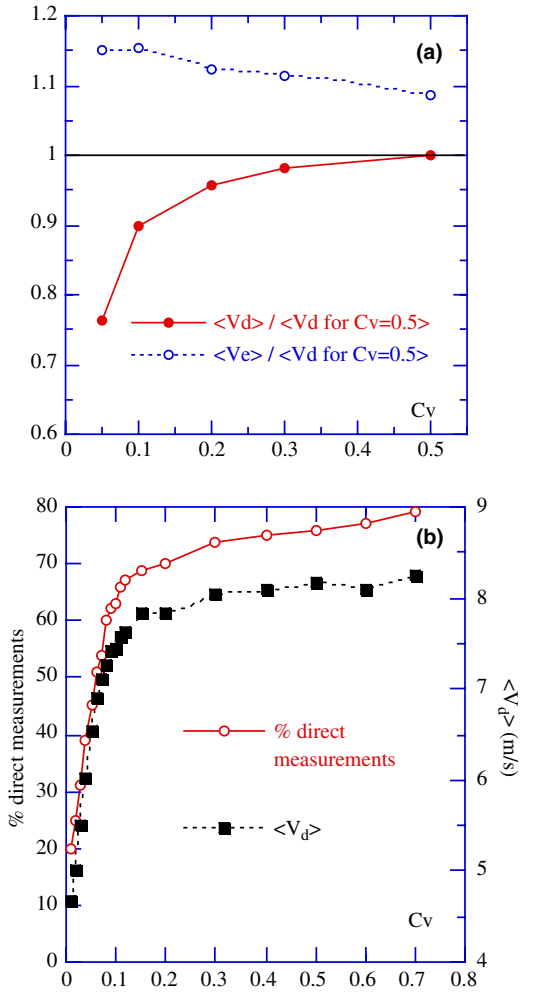

Fig. 14. (a) Comparison of the average velocities $\langle V_d \rangle$ and $\langle V_e \rangle$ and (b) evolution of the average velocity $\langle V_d \rangle$ and of the percentage of direct velocity measurements with C_V.

remains moderate. For C_V above 0.3, the deviations between the two average velocities are less than 10%. The sensitivity of the average velocity $\langle V_d \rangle$ to the parameter C_V is reported in Fig. 14b together with the evolution of the percentage N_d/N_t of direct velocity measurements. Beyond $C_V \approx 0.2$, both the average velocity and the direct measurement percentage are nearly constant: these quantities evolve within 5% when C_V ranges between 0.2 and 0.7. This is because direct velocity measurements correspond to at least 70% of the detected events. Below $C_V \approx 0.2$, both $\langle V_d \rangle$ and N_d/N_t experience important variations. Indeed, the extrapolation procedure concerns more and more events as C_V decreases. In addition, the velocity-gas dwell time relationship used for the extrapolation becomes more and more biased since it is grounded only on the largest drops (whose velocity significantly differs from the smallest ones in the present experimental conditions). The consequence is a strong underestimation of the average velocity: for $C_V \approx 0.02$, the later drops down to half its actual value while the direct validation concerns only 10% of the detected drops. In order to ensure velocity measurements that are both meaningful and weakly sensitive to the processing criteria, the default value of the coefficient C_V has therefore been set to 0.5. Although the above analysis has been performed on a single record, the selected signal is believed to be a good representative of stringent experimental conditions. In other words, no significant change in the sensitivity to C_V is to be expected with flow conditions. Note also that, in practice, the validity of the velocity estimate can directly be checked from the percentage of direct velocity measurements, or from a sensitivity analysis to C_V.

The sensitivity of the measured chord distribution to the parameter C_V has also been considered. Again, we distinguish between the detected chord distribution, as obtained from signals for which the velocity has been directly determined, and the chord pdf including the extrapolation procedure used for the smallest liquid residence times. As shown Fig. 15, the difference between the two probability density functions (pdfs) arises mainly for the smallest chords. This difference diminishes as C_V increases, due to the fact that the extrapolation applies to a smaller set of events. Finally, for the selected value of C_V, namely 0.5, the two distributions are nearly identical. From such smooth chord pdf, one can extract the size pdf $P(d)$. The corresponding procedure as well as the underlying assumptions on the flow structure are detailed elsewhere (Cartellier, 1999). Similarly, the joint size–velocity distribution $P(d, V)$ can be deduced from the joint chord–velocity distribution $P(C, V)$. However, in that case, one cannot account for the extrapolated data at small liquid residence times because of the implicitly assumed relationship between these two quantities. In practice, $P(d, V)$ will be evaluated without considering the extrapolation procedure. Such an approach is expected to be appropriate provided that direct velocity (and thus chord) measurements are performed over as least 70–75% of the detected events. Some comparisons presented in Section 5 will demonstrate that under such conditions, the measurements are indeed meaningful.

Since the liquid residence times enter the extrapolation routine, any variation in their determination could also alter the detected velocities and chords. Only the effect of C_{S2} has been investigated since this coefficient has the largest influence on T_L (see Fig. 12b). It happens that, for C_{S2} evolving between 0.1 and 0.01, the velocity pdfs are nearly unaffected and the average velocity $\langle V_e \rangle$ remains the same within 1.5%. This is because the chord–residence time correlation is almost unaffected by C_{S2}. On the opposite, the chords directly depend on the liquid residence time, and are thus slightly more affected than the velocities. Indeed, when C_{S2} is decreased down to 0.02, the corresponding pdfs are strengthened in the limit of small sizes (Fig. 16) so that the mean chord,

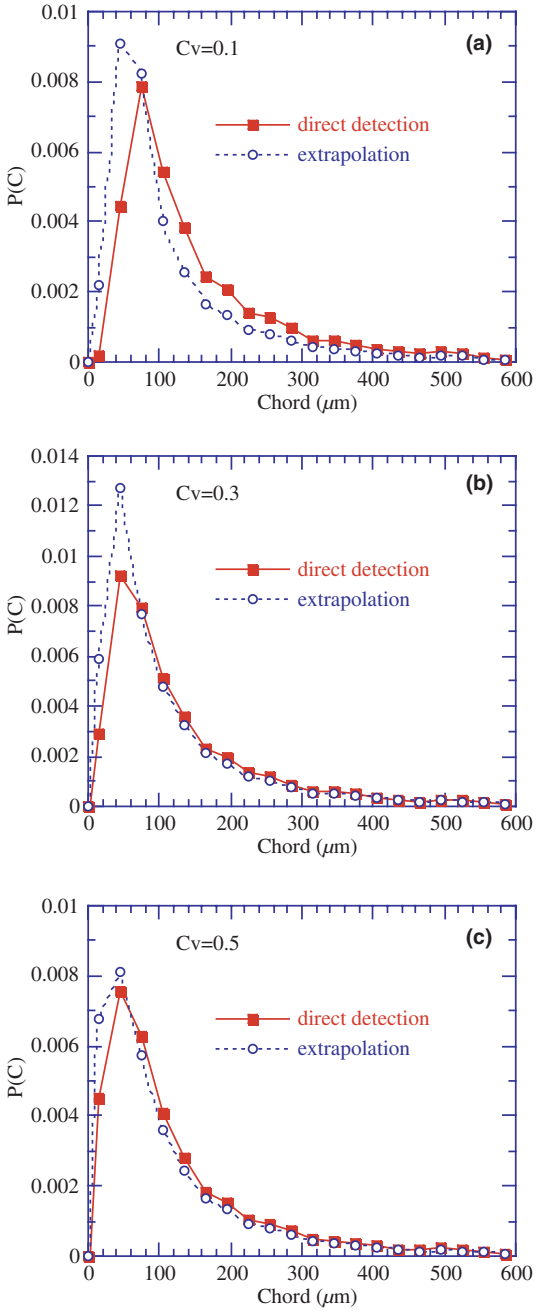

Fig. 15. Comparison between chord distributions with and without extrapolation for small liquid dwell times for different values of C_V.

which equals 135 μm with the default coefficients, diminishes by an amount close to 5%. The deviation reaches 7.5% for $C_{S2} = 0.01$ (a threshold not recommended since it is below the noise).

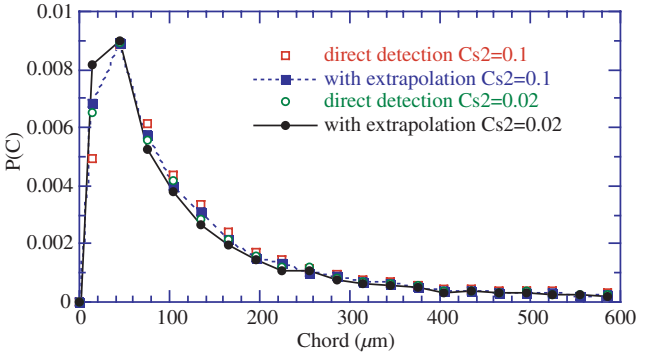

Fig. 16. Sensitivity of the chord pdf to the C_{S2} coefficient.

Yet, the influence of C_{S2} on the chords remains marginal compared with the correction due to the extrapolation procedure itself.

4.2.3. Percentage of time for the evaluation of the gas level

The last processing parameter to consider is related with the evaluation of the local level of the gas phase (A_{G2}). Let us remind that the local gas level is required for the measurements of the liquid presence time and of the transition time for every droplet signature. A_{G2} is computed as the mean value of the gas level evaluated over the first 10% of the duration of the gas plateau. A modification of this percentage can alter the liquid fraction and the average velocity. It happens that the variations on these two quantities are less than 2% for a percentage evolving between 5% and 70%. Therefore, this parameter has no influence on the measurements.

After having examined the influence of the various processing criteria, a last test deserves to be done. Indeed, from the controlled experiments presented in Section 3, it has not been possible to completely determine the range of size and velocities accessible to a given probe. Hence, it is important to evaluate the sensitivity of the measurements to the probe characteristics. In that scope, the chord pdfs detected by the two different probes have been compared for the same experimental conditions ($x/d = 1.5$, $y/d = 0.5$, $U_G = 60$ m/s, $U_L = 0.52$ m/s on the planar coaxial jet). As shown Fig. 17, the chord pdf are almost identical above about 40 μm, while significant deviations appear for smaller values. As expected, the probe[b] with the shortest latency length better detects the chords below 30 μm. In particular, both probes provide measurements in the size class centered on 5 μm, but the probe[b] detects nearly 10 times more events that probe[a]. Accordingly, the maximum of the pdf is shifted to lower sizes: it is about 20–25 μm for probe[b] and about 50–55 μm for probe[a]. These abscissa change almost in proportion the latency length variation. Despite these differences, the mean chords deduced from the two sets are the same within 10% indicating that the moments of the size pdf do not significantly depend on the sensitive head.

The proposed signal processing, with a suitable choice of the various coefficients, appears to provide fairly objective measurements of concentration, velocities and sizes. In order to fully ascertain the performances of the sensor, additional tests have been achieved in a gas–liquid co-current jet. Some results are also presented that illustrate the capacity of optical probe to provide information that is useful for model development.

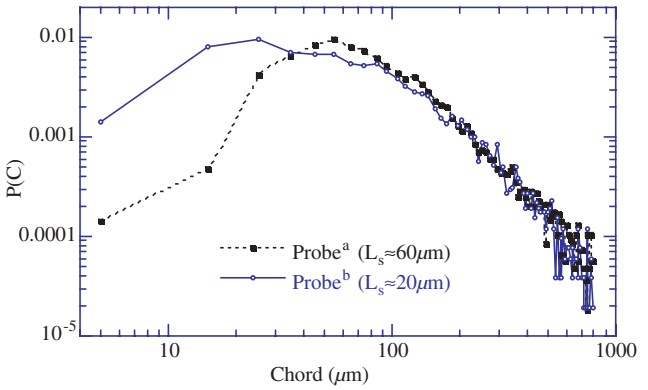

Fig. 17. Chord pdfs as detected by the two conical probes (data taken in the planar gas–liquid mixing layer at $x/D = 1.5$, $y/D = 0.5$ for $U_G = 60$ m/s, $U_L = 0.52$ m/s).

5. Probe performance in a liquid–gas mixing layer

The optical probe[b] has been used to investigate a co-current planar liquid–gas jet. The experimental facility is sketched in Fig. 18. The bottom layer is fed by water while the upper layer is a high-speed air jet. The two exhausts are rectangular sections 100 mm wide and $D/2 = 10$ mm thick (D is the hydraulic diameter). Strong contractions have been used to ensure almost uniform velocity profiles with thin, controlled boundary layers on the splitter plate. In the exit section, the mean water velocity U_L can be varied from 0.1 to 1 m/s while the mean air velocity U_G was varied between 10 and 100 m/s. The liquid Reynolds number Re_L based on the channel thickness ($Re_L = U_L D/\nu_L$ where ν_L is liquid kinematic viscosity) is of order 10^3–10^4, while the Weber number ($We = \rho_G U_G^2 D/\sigma$ where ρ_G is the gas density) varies between 26 and 3200. More details about this experiment can be found in Raynal (1997). Note that due to the presence of a liquid film flowing along the bottom wall, the lower portion of the system (namely $y/D \leqslant 0.3$) has not been scrutinized.

Previous investigations have been devoted to the analysis of the primary instability in the mixing zone. It was shown that the shear-instability of the liquid–gas interface induced the formation of liquid crests with a well defined longitudinal wavelength that is controlled by the thickness of the gas boundary layer (Raynal, 1997; Marmottant, 2001; Lasheras and Hopfinger, 2000; Marmottant and Villermaux, 2003). Such crests are thereafter destabilized and ligaments

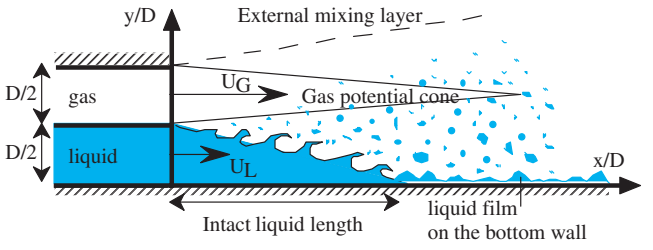

Fig. 18. Sketch of the two-dimensional gas–liquid mixing layer.

appear along the transverse direction, which subsequently break into droplets. Although this scenario is widely accepted, there is still a debate concerning the nature of the instability that leads to liquid ligaments, and also concerning the scaling law governing the ligament spacing and the drop size. Additional open questions concern the secondary atomization that may affect the spray development further downstream. In particular, breakup mechanisms related either with the turbulent stress, the mean shear or droplet collisions have been evoked to account for the observed spatial variations of the mean drop size.

5.1. Volumetric flux qualification

As a first step, the probe has been qualified in terms of volumetric flux. The reference volumetric flux J_L was evaluated with an iso-kinetic sampling technique consisting of a 10 mm I.D. straight tube facing the main flow. The water was collected through a smooth plastic tubing, which was weakly bent to minimize the pressure drop in the collecting system. When inserting this device in the flow, the change in the local gas velocity, and hence the uncertainty on the local flux, was found to be less than 10%. The reference volumetric flux was directly measured at the tube exit. With the optical probe, the local volumetric flux j_L was evaluated from the chords C_i detected for every signature according to: $j_L = \sum_{i=1\ldots N_t} C_i/T_t = (\sum_{i=1\ldots N_t} C_i/\sum_{i=1\ldots N_t} T_{Li}) \times (\sum_{j=1\ldots N_t} T_{Li}/T_t) = \alpha V_{PL}$, where V_{PL} denotes the phase average velocity. In this formula, all chords, including the extrapolated data were considered for the evaluation of j_L. These measurements were repeated at various positions, and, when integrated over the tube area, they provide the flux to be compared with the reference value. Let us mention that, for all measurements, the percentage of direct velocity measurements has never been less than 70%. The comparisons are shown Fig. 19 for three downstream sections and for various values of y/D at given injection velocities ($U_G = 60$ m/s, $U_L = 0.52$ m/s). The results from the two techniques are in good agreement, with a maximum discrepancy about 15%. The largest differences are observed in the vicinity of the bottom plate at $y = 0$, possibly due to the presence of a liquid film that alters the functioning of the sampling technique. The discrepancy is much smaller away from the liquid film, i.e. in regions where the droplets are well dispersed. In addition, various estimates of the flux have been compared. Indeed, aside the above mentioned formula based on chords, the local flux j_L was also evaluated from the joint size–velocity product density $f(\mathbf{x}, d, v)$ once the later was reconstructed. The volumetric flux density j_L equals $4/3\pi\varphi\langle R^3\rangle_f$ (respectively, $4/3\pi n\langle vR^3\rangle_f$) for uncorrelated size and velocity (respectively, for correlated size and velocity), where $\langle\bullet\rangle_f$ denotes the f weighted average of the quantity within brackets and R is the drop radius. The three estimates of j_L have been found in good agreement (deviations up to 10%) for all the conditions considered. This clearly indicates that the reconstruction process is reliable, and also that the interpolation procedure used for the smallest residence times does not affect much the measurements.

The above results provide confidence in the proposed technique. Notably, in Section 4, a single signal record was exploited that corresponded to fixed flow conditions. Here, the comparisons have been achieved for variable conditions, with a local liquid fraction evolving between 2×10^{-5} and 4×10^{-2}, a phase average velocity between 2 and 12 m/s, and a Sauter mean diameter d_{32} between 50 and 100 μm. These tests demonstrate that the uncertainty on velocity measurements remains of the same order as the one obtained under controlled piercing experiments (while the impact Weber numbers were much higher, up to 600, in the later case).

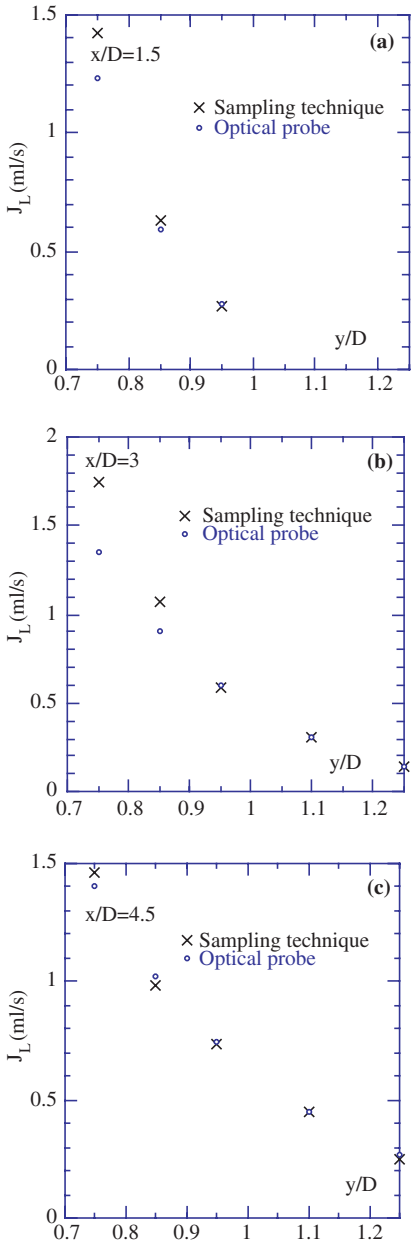

Fig. 19. Comparison of the liquid fluxes measured by the optical probe and by a sampling technique at various locations ($U_G = 60$ m/s, $U_L = 0.52$ m/s).

5.2. Dispersed phase characteristics resulting from primary atomization

To illustrate the potentiality of optical probes for the investigation of sprays, some results gathered in the two-dimensional gas–liquid mixing layer are now briefly presented. Various

quantities are of key importance for the modeling of sprays. Hereafter, emphasis is placed on the evolution of the drop characteristics with the gas velocity when the dynamic pressure ratio ($M = \rho_G U_G^2/\rho_L U_L^2$) is held constant. Indeed, the parameter M has been shown to control the liquid intact length, the later being about $6D \times M^{-1/2}$ for high M (Raynal, 1997). In order to be representative of the primary atomization mechanisms, the measuring location was set just above the end of the liquid intact length (namely $x/D = 1.5$, $y/D = 0.5$).

5.2.1. Drop sizes

The size pdfs were deduced from the chord distributions assuming that all liquid lumps are treated as contributions due to spherical droplets. In the reconstruction procedure (for details see Liu and Clark, 1995; Cartellier, 1999 for example), corrections are incorporated for the effective probe volume that evolves with the drop size. In addition, the actual size distributions $P(d)$ were evaluated for size and velocity either correlated or uncorrelated (Cartellier, 1999). Indeed, since the drops formed in the primary atomization zone are accelerated by the gas stream, a strong correlation between size and velocity is expected. However, the turbulence intensity is quite strong in a mixing layer, not mentioning the large scale vortical structures that form nor the possible collisions between inclusions, and this would cause at least a partial decorrelation between sizes and velocities. It was thus decided to consider both hypotheses for the size reconstruction. Two moments of the size distributions, namely the arithmetic mean d_{10} and the Sauter mean diameters d_{32} are given Fig. 20 versus the air injection velocity U_G for $M = 16$. It is seen that the two assumptions lead to very similar results, with slightly smaller drops when size and velocity are assumed correlated. The trends shown in Fig. 20 are consistent with available results. In particular, the existence of two regimes, respectively, below and above $U_G = 30$ m/s, has been already recognized (Lasheras and Hopfinger, 2000). At small gas velocities (i.e. for *We* less than about hundred), a capillary instability of the liquid rim is expected to hold. That scenario leads to $d_{10} \propto \sigma/\rho_G U_G^2$ in agreement with the trend shown Fig. 20. At larger velocities, previous experi-

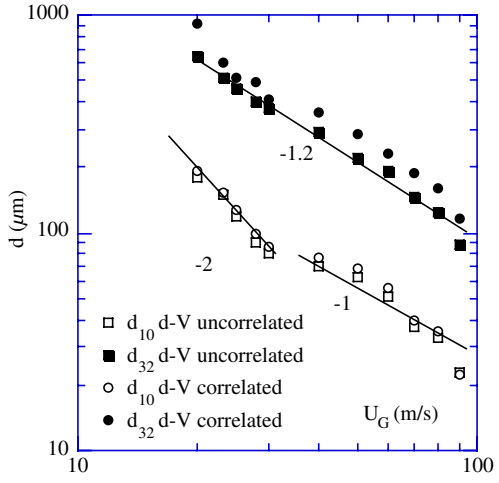

Fig. 20. Mean drop size evolutions with the gas velocity at a constant dynamic pressure ratio ($M = \rho_G U_G^2/\rho_L U_L^2 = 16$). Measurements were made at $y/D = 0.5$, $x/D = 1.5$, i.e. above the end of the liquid intact length.

ments performed on coaxial atomizers, either using imaging techniques or phase Doppler anemometry, indicate that d_{10} evolves as U_G^{-1} (Marmottant, 2001; Varga, 2002) and d_{32} varies as $U_G^{-1.3}$ (Varga, 2002). All these trends agree with the drop sizes measured with the optical probe. The implications of these scaling laws with respect to the interfacial instability are discussed elsewhere (Hong et al., 2002).

5.2.2. Others spray characteristics

Aside the drop size, many others quantities are of importance for applications or are needed to provide appropriate boundary conditions for numerical simulations, but these have been scarcely measured. The number density n and its flux φ for instance, obtained under the same experimental conditions, are reported in Fig. 21a. Both show a very strong increase with U_G. These two quantities are related by the dispersed phase mean velocity $\langle v\rangle_f$ since $\varphi = n\langle v\rangle_f$. When size and velocity are not correlated, $\langle v\rangle_f$ equals the phase average velocity V_{PL} (otherwise $V_{PL} = \langle vR^3\rangle_f/\langle R^3\rangle_f$ and it could slightly differ from $\langle v\rangle_f$). From the observed trends, it is seen that $\langle v\rangle_f$ remains proportional to the gas injection velocity (this statement holds for a fixed position and for constant M). This trend is confirmed by the velocity measurements performed with the optical probe as shown in Fig. 21b. In addition, assuming a directional flow and from kinematic considerations only (Zuber and Findlay, 1965), the local dispersed phase fraction is related to the volumetric liquid phase fraction $\beta = U_L/(U_G + U_L)$ (the cross sections are identical here) by

$$\alpha/\beta = 1/[C_0 + C_1 V_r/U_G]$$

where V_r is the mean relative velocity between phases. The coefficients C_0 and C_1 depend only on the velocity and concentration profiles, and are assumed not to vary. For a fixed M, β remains constant. Since the experiments have shown that the dispersed phase velocity is proportional to U_G, V_r/U_G does not change. Consequently, the local dispersed phase fraction α should not evolve

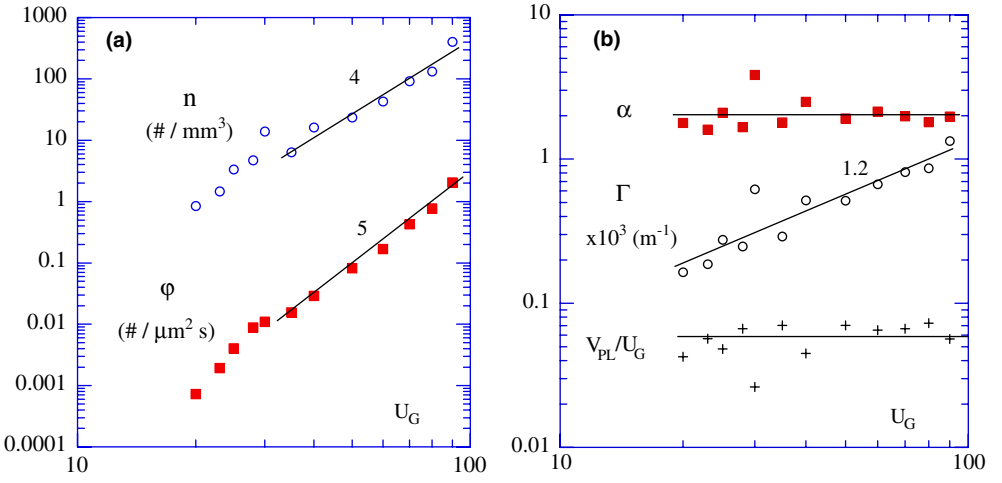

Fig. 21. Evolution with the gas velocity, at $M = 16$, of: (a) the number density n and its flux φ and (b) the dispersed phase fraction α, the interfacial area density Γ and the phase average velocity V_{PL} scaled by U_G. Measurements made at $y/D = 0.5$, $x/D = 1.5$, i.e. above the end of the liquid intact length.

when U_G varies. This is indeed what is measured with the probe (Fig. 21b). Moreover, since the interfacial area density is given by $6\,\alpha/d_{32}$ provided that the inclusions remain convex, it happens that, at a given position and for M constant, Γ is controlled by the Sauter mean diameter and not by the dispersed phase concentration. The trend shown Fig. 21b indeed corresponds to $\Gamma \sim d_{32}^{-1}$ From a practical view point, although the fluxes strongly increase with the gas velocity, the gain in terms of surface of exchange is much more limited: it is mainly controlled by the interfacial instability that governs the size of liquid inclusions.

Although refinements can be made, the above results demonstrate that the conical probe is indeed able to provide consistent data. In particular, the relevant secondary atomization mechanism can be identified from an analysis of the spray evolution. Preliminary results in that direction are discussed in Hong et al. (2002). More generally, a comparison of the dispersed phase characteristics as measured by a conical probe with predictions from numerical simulations would be quite useful to improve the modeling of dispersion, break-up and coalescence effects in such sprays.

6. Conclusion

Experiments performed under controlled conditions as well as in actual sprays have demonstrated that conical optical probes are suitable for drop detection over a significant range of sizes and velocities. Chords and velocities can be detected for droplets as small as about one fourth to one fifth of the probe sensitive length. The typical uncertainties, including the influence of impact conditions, are about 10% for chords and 20% for velocities. A reliable signal processing has been developed and has been proved fairly objective. When applied to a spray produced by planar co-flowing jets, the sensor has proved its ability to obtain significant information concerning notably the joint size–velocity pdf, the dispersed phase fraction and the interfacial area density. Such variables are required for the development of reliable two-phase flow models. This sensor is thus a promising tool to characterize sprays involving strongly distorted droplets and dense sprays where techniques such as PDA fail. Concerning the main limitations of the technique, it seems mandatory for the flow to have a strong preferred direction. Also, while the moments of the size pdf have been shown not to depend on the probe design, the later affects the size pdfs in the limit of very small drops. This influence deserves to be more thoroughly investigated, but, from available data, one can be confident in the pdf down to sizes of the order of half the probe latency length. In the same prospect, the average dispersed phase characteristics may become less accurate as the size distribution shifts to smaller droplets. The precise limits of the proposed technique remain to be determined, having also in mind that optical probes of smaller sensitive length can be manufactured.

Acknowledgements

The authors would like to acknowledge SNECMA for its financial support provided under Grant No. 2001-38G.

References

Barrau, E., Rivière, N., Poupot, Ch., Cartellier, A., 1999. Single and double optical probes in air-water two-phase flows: real time signal processing and sensors performances. Int. J. Multiphase Flow 25, 229–256.

Carreau, J.L., Porcheron, E., Le-Visage, D., Prevost, L., Roger, F., 1997. Liquid core characterization of coaxial liquid oxygen/inert gas jets. Int. J. Fluid Mech. Res. 24, 498–507.

Cartellier, A., 1990. Optical probes for local void fraction measurements: characterization of performances. Rev. Sc. Instrum. 61 (2), 874–886.

Cartellier, A., 1999. Post-treatment for phase detection probes in non-uniform two-phase flows. Int. J. Multiphase Flow 25, 201–228.

Cartellier, A., Achard, J.-L., 1991. Local phase detection probes in fluid/fluid two-phase flows. Rev. Sci. Instrum. 62, 279–303.

Cartellier, A., Barrau, E., 1998a. Monofiber optical probes for gas detection and gas velocity measurements: conical probes. Int. J. Multiphase Flow 24, 1265–1294.

Cartellier, A., Barrau, E., 1998b. Monofiber optical probes for gas detection and gas velocity measurements: optimised sensitive tips. Int. J. Multiphase Flow 24, 1295–1315.

Dias, S.G., França, F.A., Rosa, E.S., 2000. Statistical method to calculate local interfacial variables in two-phase bubbly flows using intrusive crossing probes. Int. J. Multiphase Flow 26, 1797–1830.

Hibiki, T., Ishii, M., Xiao, Z., 2001. Axial interfacial area transport of vertical bubbly flows. Int. J. Heat Mass Transfer 44, 1869–1888.

Hong, M., Cartellier, A., Hopfinger, E.J., 2000. Spray characterization using optical probes: feasibility of droplet velocity, size and concentration measurements. In: Proceedings of the 2nd European–Japanese Two-Phase Flow Group Meeting, Tsukuba, September 25–29, Japan.

Hong, M., Cartellier, A., Hopfinger, E.J., 2002. Atomization and mixing in coaxial injection. In: Proceedings of the 4th International Conference on Launcher Technology "Space Launcher Liquid Propulsion", Liège, Belgium, December 3–6.

Kataoka, I., Ishii, M., Serizawa, A., 1986. Local formulation and measurements of interfacial area concentration. Int. J. Multiphase Flow 12, 505–527.

Lasheras, J.C., Hopfinger, E.J., 2000. Liquid jet instability and atomization in a coaxial gas stream. Annu. Rev. Fluid Mech. 32, 275–308.

Lasheras, J.C., Villermaux, E., Hopfinger, E.J., 1998. Break-up and atomization of a round water jet by a high-speed annular air jet. J. Fluid Mech. 357, 351–379.

Li, J., Lopez-Pagés, E., Yecko, Ph., Zaleski, S., 2004. Droplet formation in sheared liquid–gas layers. Theor. Comp. Fluid Dyn. submitted.

Liju, P.-Y., Machane, R., Cartellier, A., 2001. Surge effect during the water exit of an axisymetric body travelling normal to a plane interface: experiments and BEM simulation. Exp. Fluids 31, 241–248.

Lin, S.P., Reitz, R.D., 1998. Drop and spray formation from a liquid jet. Annu. Rev. Fluid Mech. 30, 85–105.

Liu, W., Clark, N., 1995. Relationships between distributions of chord lengths and distributions of bubble size including their statistical parameters. Int. J. Multiphase Flow 21, 1073–1089.

Marmottant, Ph., 2001. Atomisation d'un liquide par un courant gazeux. Thèse de Doctorat, Inst. Nat. Polytechnique, Grenoble.

Marmottant, Ph., Villermaux, E., 2003. Atomisation primaire dans les jets coaxiaux. Combustion 2, 89–125.

Porcheron, E., 1998. Atomisation d'un jet liquide par un jet de gaz inerte appliquée à la propulsion cryotechnique. Thèse de Doctorat, Univ. de Poitiers, France.

Raynal, L., 1997. Instabilité et entraînement à l'interface d'une couche de mélange liquide-gaz. Thèse de Doctorat, Univ. Joseph Fourier, Grenoble.

Tishkoff J.M., Ingebo R.D., Kennedy J.B. (Eds.), 1984. Liquid Particle Size Measurement Techniques, ASTM Special Technical Publication 848.

Vallet, A., Burluka, A., Borghi, R., 2001. Development of an Eulerian model for the "atomization" of a liquid jet. Atomisat. Spray 11, 521–544.

Varga, C., 2002. Initial break-up of small diameter liquid jet by a high speed gas stream. Ph.D. Thesis, UCSD, USA.

Williams, F.A., 1985. Combustion Theory, second ed. Addison-Wesley, Reading, MA.
Yecko, Ph., Zaleski, S., Fullana, J.-M., 2002. Viscous modes in two-phase mixing layers. Phys. Fluids 14, 4115–4122.
Zuber, N., Findlay, J.A., 1965. Average volumetric concentration in two-phase flow systems. J. Heat Transfer (November), 453–468.
Zûn, I., Filipic, B., Perpar, M., Bombac, A., 1995. Phase discrimination in void fraction measurements via genetic algorithms. Rev. Sc. Instrum. 66, 5055–5064.